Electrically Actuated Microbeams: An Explicit Calculation of the Coulomb Integral in the Entire Stable and Unstable Regimes Using a Chebyshev-Edgeworth Approach

Hermann A.G. Schenk,[1,*] Anton Melnikov⊙,[2] Franziska Wall,[2] Matthieu Gaudet⊙,[3] Michael Stolz,[2,4] David Schuffenhauer,[2] and Bert Kaiser[2]

[1]*Arioso Systems GmbH, Dresden 01109, Germany*

[2]*Fraunhofer Institute for Photonic Microsystems IPMS, Dresden 01109, Germany*

[3]*Department für Informatik—AMiR, Universität Oldenburg, Oldenburg 26111, Germany*

[4]*Brandenburg University of Technology Cottbus-Senftenberg, Cottbus 03046, Germany*

In this paper we present an analytical model for large displacements of electrostatically actuated elastic microbeams, including all their stable and unstable states. Such microbeams are the core element of microelectromechanical system-based resonators, transducers, and actuators. Their accurate modeling is essential to their development. Especially in the realm of system design, there is a need for lumped-parameter models with a single degree of freedom, where a large number of such subsystems can interact with each other. The state of the art suggests using zero-mode approximations far from the pull-in limit or using multi-degree-of-freedom Galerkin projection to get the results close to the pull-in limit. The challenges of finding a closed-form solution lie in the complicated structure of the Coulomb integral. Our approach to evaluating this integral is based on a Chebyshev-Edgeworth-type method common in analytic probability theory and allows the states to be accurately modeled where the kernel is close to the singularity. Although this approach to nonlinear dynamical systems is used here for a very specific purpose, where we report a user-friendly closed solution of a clamped-clamped microbeam, it has a much broader scope. It is apt to analyze different boundary conditions, electrostatic fringe field corrections, and squeeze film damping, to name a few applications. Moreover, the method presented here can generally be applied to the evaluation of singular integral kernels.

I. INTRODUCTION

Coulomb-actuated microbeams play a crucial role in many microelectromechanical system (MEMS) applications [1–3]. They enable actuation using electrostatic forces and capacitive sensing, give rise to pioneering applications in medicine [4], communications [5,6], sensing [2,7], and consumer products [8–12]. To meet the needs of recent developments, such as the 5G Internet of Things [6], augmented reality [13], and green information and communications technology (ICT) [14,15], a system level consideration of a high number of electromechanical components is necessary. This is only possible, if accurate and highly efficient lumped-parameter models (LPMs) of the components are available.

In this paper we systematically derive a single degree of freedom LPM, describing the physics of prismatic clamped-clamped Coulomb actuated microbeams with high precision as compared to FEM simulations and in line with experimental findings. In a previous publication, Melnikov *et al.* [16] demonstrated that the stable and unstable states of prismatic Coulomb actuated Euler-Bernoulli microbeams, clamped at both ends, can be successfully simulated combining FEM with arc-length solvers. The resulting model predictions were experimentally scrutinized by combining direct optical observations with a modal analysis regarding Euler-Bernoulli eigenmodes. Both approaches revealed convincing evidence for an almost perfect congruence of the respective bending profile and the shape of the lowest Euler-Bernoulli eigenmode (the zero mode, also called the main or first deflection mode). It was shown that this is true for the entire applicable voltage range including the pull-in regime within very small error margins. This does not sound

---

*hermann.schenk@arioso-systems.com

surprising given the zero-mode approximations in the literature for the regimes far from the pull-in boundary [17–19], however the observation mentioned above [16] suggests the possibility of accurately modeling the physics close to the pull-in limit or even beyond. This implies a lumped-parameter model with a single degree of freedom, amenable to direct physical interpretation, opening possibilities in modeling and understanding microbeam statics and dynamics. The final result including single degree of freedom equations is separately formulated in Sec. III E.

II. BASIC EQUATIONS

Studies analytically deriving lumped-parameter models, e.g., Nayfeh, Younis, and Rahman [19–25] typically begin with the nonlinear Euler-Bernoulli beam equation for the bending profile $w(\xi, \tau)$. In its dimensionless form used by Nayfeh *et al.* [24] this equation reads

$$\frac{\partial^2 w}{\partial \tau^2} + c \frac{\partial w}{\partial \tau} + \frac{\partial^4 w}{\partial \xi^4} = (\gamma[w] + N) \frac{\partial^2 w}{\partial \xi^2} + \alpha_2 \frac{v(\tau)^2}{(1 - w)^2}. \tag{1}$$

Here ξ and τ are the dimensionless beam coordinate and the dimensionless time. The dynamic damping coefficient is denoted by c. The geometry-dependent parameters α_1 and α_2 are given in Eq. (47) below. N is a dimensionless axial stress and $v(\tau)$ is the dimensionless drive voltage. The beam is assumed to be clamped at $\xi = -\frac{1}{2}$ and at $\xi = +\frac{1}{2}$, where the usual clamped-clamped boundary conditions Eq. (A7) apply. The nonlocal functional $\gamma[w]$ models the stress stiffening of the clamped-clamped beam,

$$\gamma[w] = \alpha_1 \int_{-(1/2)}^{+(1/2)} \left(\frac{\partial w}{\partial \xi} \right)^2 d\xi. \tag{2}$$

Nayfeh *et al.* expand the bending profile with respect to a complete orthonormal Hilbert-space base $\psi_n(\xi)$,

$$w(\xi, \tau) = \sum_{n=0}^{\infty} \hat{w}_n(\tau) \psi_n(\xi). \tag{3}$$

Upon insertion into Eq. (1), the partial differential equation (1) is converted into an infinite set of coupled nonlinear ordinary differential equations of the form [19–25]

$$\frac{\partial^2 \hat{w}_n}{\partial \tau^2} + c \frac{\partial \hat{w}_n}{\partial \tau} + \sum_{m=0}^{m=\infty} k_{n,m}[w] \hat{w}_m = \alpha_2 v^2 F_n[\tau, w]. \tag{4}$$

Unlike Nayfeh *et al.*, we select $\{\lambda_n, \psi_n(\xi)\}_{n \in \mathbb{N}}$ to be the Euler-Bernoulli eigensystem and can therefore be a little

more specific,

$$k_{n,m}[w] = \lambda_n \delta_{n,m} + (\gamma[w] + N) \chi_{n,m}, \tag{5}$$

$$\chi_{n,m} = \int_{-(1/2)}^{+(1/2)} \frac{\partial \psi_n}{\partial \xi} \frac{\partial \psi_m}{\partial \xi} d\xi. \tag{6}$$

The challenge with this approach however is that the resulting stiffness matrix $k_{n,m}[w]$ and the force components $F_n[\tau, w]$ are rather intricate, nonlinear, singular, and time-dependent functionals of the entire infinite set of the coefficient functions $\{\hat{w}_n(\tau)\}_{n \in \mathbb{N}}$:

$$\begin{aligned} k_{n,m}[w] &= k_{n,m}[\hat{w}_0(\tau), \ldots, \hat{w}_n(\tau), \ldots], \\ F_n[\tau, w] &= F_n[\tau, \hat{w}_0(\tau), \ldots, \hat{w}_n(\tau), \ldots]. \end{aligned} \tag{7}$$

This circumstance makes it in general very challenging to obtain any elucidating results from Eq. (4). As can be see from the literature, the complexity of the functionals $k_{n,m}[w]$ and $F_n[\tau, w]$ leads to a tedious computational task, even after introducing well-considered simplifications, e.g., see Younis *et al.* [19]. The resulting computations seem neither more attractive than direct numerical methods, nor is the need for the number of degrees of freedom, required to obtain satisfactory accuracy, amenable to direct physical interpretation. In fact the number of modes required in Nayfeh *et al.*'s approach turns out to be an artefact, essentially reflecting their comparatively straight forward attempt to technically cope with the singular nature of the Coulomb force, as we see. The picture substantially changes however with the observation of Melnikov *et al.* [16] that the lowest Euler-Bernoulli eigenmode $\psi_0(\xi)$ is by far dominating the physics of Coulomb actuated prismatic clamped-clamped microbeams in practical applications. This observation implies that the use of higher modes in a LPM for a prismatic Euler-Bernoulli beam is hardly justified, unless higher kinetic energies are involved. Due to the large spectral distance, typically a multiple of the elastic energy corresponding to the considered deflection of the zero mode is required for significant effects involving higher modes.

The observation of Melnikov *et al.* [16] essentially allows Eq. (3) to be reduced to the single term

$$\begin{aligned} w(\xi, \tau) &\approx z(\tau) \frac{\psi_0(\xi)}{\psi_0(0)}, \quad 0 \leq z(\tau) \leq 1, \\ \psi_0(\xi) &= \frac{\cosh(\beta_0 \xi)}{\cosh(\beta_0/2)} - \frac{\cos(\beta_0 \xi)}{\cos(\beta_0/2)} \end{aligned} \tag{8}$$

since the contribution of the higher modes is negligibly small. Here β_0 is the smallest solution to the equation

$$0 = \tanh(\beta/2) + \tan(\beta/2). \tag{9}$$

In zero-mode approximation, Eq. (4) simplifies to the quite handy form

$$\frac{\partial^2}{\partial \tau^2}z + c\frac{\partial}{\partial \tau}z + k_0 z + \kappa z^3 = u^2 f_0(z). \qquad (10)$$

The parameters κ, k_0, and u are defined as

$$\kappa = \alpha_1 \left(\frac{\chi_0}{\psi_0(0)}\right)^2, \qquad (11)$$

$$k_0 = \lambda_0 + N\chi_0, \quad u = \psi_0(0)\sqrt{\alpha_2}v,$$

$$\chi_0 = \int_{-(1/2)}^{+(1/2)} \left(\frac{\partial \psi_0}{\partial \xi}\right)^2 d\xi \qquad (12)$$

and the force term is

$$f_0(z) = \int_{-(1/2)}^{+(1/2)} \frac{(\psi_0(\xi)/\psi_0(0))}{[1 - z(\psi_0(\xi)/\psi_0(0))]^2} d\xi. \qquad (13)$$

The remaining key challenge, and the prime topic of this paper, is of course evaluating the Coulomb integral $f_0(z)$. This requires a nonpertubative treatment of the Coulomb singularity. The ad hoc approach of Younis *et al.* [19] essentially creates an artificial need for higher modes and therefore enforces dealing with a coupled system of non-linear ordinary differential equations (ODEs). This is far from satisfactory. It is the purpose of this paper to demonstrate, in contrast, that the physics of a Coulomb actuated prismatic Euler-Bernoulli is contained in the single ODE, Eq. (10), to an extent sufficient for most practical purposes in MEMS technology. To this end, we devise a nonpertubative strategy of dealing with the Coulomb integral, based on a Chebyshev-Edgeworth-type expansion [26,27]. As a result we arrive at a highly accurate analytical expression for $f_0(z)$. Finally, the application of our zero-mode LPM, Eq. (47), to the simulation results and experimental findings of Melnikov *et al.* [16], reveal a very good agreement.

III. RESULTS

A. Chebyshev's argument

Our evaluation of the integral $f_0[z]$ begins with the series representation

$$f_0(z) = \sum_{n=1}^{\infty} n I_n z^{n-1}, \qquad (14)$$

where the integrals I_n are defined as

$$I_n = \int_{-(1/2)}^{+(1/2)} \left(\frac{\psi_0(\xi)}{\psi_0(0)}\right)^n d\xi. \qquad (15)$$

Note that because $|I_n| < 1$ we can infer by means of the Cauchy-Hadamard theorem [28] that the series Eq. (14) is

absolutely convergent in the open disc $|z| < 1$, as required for our purposes. The integrals I_n can be cast into the form,

$$I_n = \frac{\sqrt{2\pi}}{\sigma\sqrt{n}} \int_{-(1/2)\sigma\sqrt{n}}^{+(1/2)\sigma\sqrt{n}} \Phi_n(\xi)d\xi, \qquad (16)$$

where $\Phi_n(\xi)$ is defined as

$$\Phi_n(\xi) = \frac{1}{\sqrt{2\pi}} \left(\frac{1}{\psi_0(0)}\psi_0\left(\frac{\xi}{\sigma\sqrt{n}}\right)\right)^n,$$

$$\sigma^2 = -\frac{\psi_0^{(2)}(0)}{\psi_0(0)}. \qquad (17)$$

Our strategy now is to evaluate the limiting function $\Phi_\infty(\xi)$ of the sequence $\{\Phi_n(\xi)\}_{n\in\mathbb{N}}$ and subsequently to expand $\Phi_n(\xi)$ around $n = \infty$ with respect to n^{-1}. This allows us to explicitly perform the integration Eq. (16). As a result we can perform the summation Eq. (14). This way we arrive at the targeted formula for $f_0(z)$.

The crucial observation regarding the limiting function $\Phi_\infty(\xi)$ is that the sequence $\{\Phi_n(\xi)\}_{n\in\mathbb{N}}$ uniformly converges to the shape of the Gauss bell curve,

$$\lim_{n\to\infty} \Phi_n(\xi) = \frac{1}{\sqrt{2\pi}}\exp\left(-\frac{\xi^2}{2}\right). \qquad (18)$$

This fact is illustrated in Fig. 1. To motivate how this comes about, we remind the reader of Euler's elementary definition of the exponential function, presented here in a form suitable for our purposes,

$$\lim_{n\to\infty} \frac{1}{\sqrt{2\pi}}\left(1 - \frac{\xi^2}{2n}\right)^n = \frac{1}{\sqrt{2\pi}}\exp\left(-\frac{\xi^2}{2}\right). \qquad (19)$$

The quite perplexing idea that Eq. (19) holds for a much broader class of functions, inserted into its left-hand side, dates back to the ground-breaking contributions of Chebyshev to the field of analytical probability theory [26]. In fact Eqs. (18) and (19) essentially are special a case of the celebrated central limit theorem (CLT). The reader acquainted with the CLT is reminded that the operations of multiplication and convolution in function space interchange their roles when subjected to a Fourier transformation. There is however no need to discuss the details of the proof of the CLT here: luckily, our mechanical setting allows for a pedestrian approach to verify Eq. (18).

The proof starts with the observation that the normalized bending profile of a fully concentrated load (only the right-hand side of the symmetric profile is given),

$$g(\xi) = (1 - 2\xi)^2(1 + 4\xi), \quad 0 \le \xi \le \frac{1}{2} \qquad (20)$$
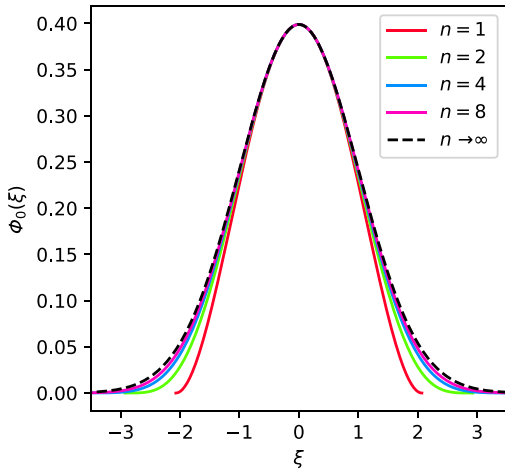
FIG. 1. $\Phi_n(\xi)$ is compared for $n = 1, 2, 4, 8$ (colored lines) to the Gauss bell curve (dashed black line) illustrating the rapid convergence according to Eq. (18).

and the normalized bending profile of the fully distributed, i.e., constant load,

$$h(\xi) = \left(1 - 4\xi^2\right)^2 \tag{21}$$

provide an upper and a lower bound for $\phi_n(\xi)$,

$$G_n(\xi) \geq \phi_n(\xi) \geq H_n(\xi). \tag{22}$$

Here $G_n(\xi)$ and $H_n(\xi)$ are defined analogously to Eq. (17), i.e., by replacing $g(\xi)$ and $h(\xi)$, respectively, for $\psi_0(\xi)$ in that equation (also the respective σ needs to be calculated),

$$G_n(\xi) = \frac{1}{\sqrt{2\pi}} \left(1 - \frac{\xi}{\sqrt{6n}}\right)^{2n} \left(1 + \frac{2\xi}{\sqrt{6n}}\right)^n,$$
$$H_n(\xi) = \frac{1}{\sqrt{2\pi}} \left(1 - \frac{\xi^2}{4n}\right)^{2n}. \tag{23}$$

The relation Eq. (22) is easily verified by establishing the assertion for $n = 1$ first, and then using the positivity of the functions involved when raising to the nth power. Note that the relation Eq. (22) also is invariant under the scaling of the ξ axis, required when progressing from n to $n + 1$. Computing the limiting function of the sequence $\{H_n(\xi)\}_{n\in\mathbb{N}}$ is a simple application of Eq. (19),

$$\lim_{n\to\infty} H_n(\xi) = \lim_{n\to\infty} \frac{1}{\sqrt{2\pi}} \left(1 - \frac{\xi^2}{4n}\right)^{2n}$$
$$= \lim_{m\to\infty} \frac{1}{\sqrt{2\pi}} \left(1 - \frac{\xi^2}{2m}\right)^m$$
$$= \frac{1}{\sqrt{2\pi}} \exp\left(-\frac{\xi^2}{2}\right). \tag{24}$$

Computing the limiting function of the sequence $\{G_n(\xi)\}_{n\in\mathbb{N}}$ is a little more challenging,

$$\lim_{n\to\infty} G_n(\xi) = \lim_{n\to\infty} \frac{1}{\sqrt{2\pi}} \left(1 - \frac{\xi^2}{2n} + \frac{\xi^3}{3\sqrt{6n^3}}\right)^n$$
$$= \lim_{n\to\infty} \frac{1}{\sqrt{2\pi}} \left(1 - \frac{\xi^2}{2n}\right)^n \left(1 + O\left(\frac{1}{n}\right)\right)^{(1/2)}$$
$$= \frac{1}{\sqrt{2\pi}} \exp\left(-\frac{\xi^2}{2}\right). \tag{25}$$

Dini's theorem [29] asserts the uniformity of the convergence in both cases. Now since both, the upper and the lower bound of $\Phi_n(\xi)$ uniformly converge to the Gaussian, the same holds true for the sequence $\{\Phi_n(\xi)\}_{n\in\mathbb{N}}$ itself, establishing Eq. (18).

Before ending this section, we would like to highlight that Chebyshev's general argument works in the domain of elastomechanics far beyond the simple case presented here and does not require any kind of symmetry. That is because Chebyshev essentially exploits the fact that Hermite polynomials form a complete base of the Hilbert space of functions over the reals, that are square integrable with respect to the measure defined by the Gauss bell curve.

B. The Edgeworth expansion

For the evaluation of the Coulomb integral $f_0(z)$ we need to know how exactly $\Phi_n(\xi)$ approaches Gauss' bell curve as n grows larger. The answer is provided by the famous Edgeworth expansion: following the ideas of Edgeworth, Eq. (18) warrants the existence of an asymptotic expansion of the form [27,30]

$$\Phi_n(\xi) = \frac{1}{\sqrt{2\pi}} \exp\left(-\frac{\xi^2}{2}\right)$$
$$\times \left(1 - \frac{c_1(\xi)}{n} + \frac{c_2(\xi)}{n^2} + O\left(\frac{1}{n}\right)^3\right). \tag{26}$$

The explicit version of this asymptotic expansion, is obtained by expanding $\Phi_n(\xi)$ in a Taylor series at $n = \infty$ in powers of n^{-1}. The computation of the respective Taylor coefficients is enabled by the use of Eq. (18) and of

$$\sqrt{2\pi}\,\Phi_1(\xi) = 1 - \frac{\xi^2}{2} + \frac{\mu_4\xi^4}{24} - \frac{\mu_6\xi^6}{720} + O(\xi)^8. \tag{27}$$

Here we introduce the following abbreviations related to the derivatives of order $2k$:

$$\mu_{2k} = \frac{(-1)^k}{\sigma^{2k}} \frac{\psi_0^{(2k)}(0)}{\psi_0(0)}, \tag{28}$$

$$\mu_{4k} = \mu_{4k+2} = \left(\frac{\cosh(\beta_0/2) - \cos(\beta_0/2)}{\cosh(\beta_0/2) + \cos(\beta_0/2)} \right)^{2k}. \quad (29)$$

The sequence of integers appearing in Eq. (27) is the sequence of the nonprime factorials; this jointly with Eq. (29) implies that the expansion Eq. (27) is absolutely convergent within an infinite radius of convergence. Merten's theorem regarding Cauchy products [31] therefore ensures that any integer power of Eq. (27), required for the evaluation of Eq. (17) exists, also possessing an infinite radius of convergence.

The first two coefficients of the Edgeworth expansion obtained following the route outlined here are

$$c_1(\xi) = \frac{-3 + \mu_4}{24} \xi^4,$$

$$c_2(\xi) = \frac{(-3 + \mu_4)^2}{1152} \xi^8 + \frac{-30 + 15\mu_4 - \mu_6}{720} \xi^6. \quad (30)$$

Finally we would like to add that in the setting of analytical probability theory, the $\Phi_1(\xi)$ plays the role of the characteristic function of a probability density and the $\{\mu_n\}_{n\in\mathbb{N}}$ are its respective moments. In our case, the Fourier transform of $\Phi_1(\xi)$, which should be a probability density, can adopt negative values. It only is asymptotically a non-negative function. So the notions of analytical probability theory, strictly speaking, do not apply. However the line of arguments of Chebyshev and Edgeworth still hold under our somewhat weaker conditions, as we explicitly show above.

C. Evaluating the Coulomb integral

In this section we evaluate Eq. (16) and perform the summation Eq. (14). The last subtlety to cope with, are the finite boundaries of the integral Eq. (16). While it is perfectly possible to analytically perform the integration within these finite boundaries and expand the results in terms of n^{-1}, little is gained by this tedious exercise. Truncating the integrand at order $O(n)^{-3}$ according to Eq. (26) and extending the integration boundaries of Eq. (16) to infinity generates an overall error, which is negligible for all practical purposes, as we show in Eq. (33) below. Therefore, we evaluate Eq. (16) in the form,

$$I_n = \frac{\sqrt{2\pi}}{\sigma\sqrt{n}} \int_{-\infty}^{+\infty} \Phi_n(\xi) \, d\xi \pm \bar{\Delta}_n. \quad (31)$$

Inserting Eqs. (26) and (30) into Eq. (31) yields

$$I_n = \frac{\sqrt{2\pi}}{\sigma} \times \left(\frac{1}{n^{(1/2)}} + \frac{\mu_4 - 3}{8n^{3/2}} \right.$$

$$\left. + \frac{75 - 90\mu_4 + 35\mu_4^2 - 8\mu_6}{384n^{5/2}} \right) + \Delta_n, \quad (32)$$

where the remainder Δ_n in Eq. (32) accounts for both simplifications mentioned above. An upper bound for Δ_n can easily be found upon noticing that the maximum remainder occurs for $n = 2$. Taylor's remainder theorem then asserts that according to Eqs. (26) and (31) the remainder decays at least with the power $n^{5/2}$,

$$0 < \Delta_n \le \Delta_2 \left(\frac{2}{n} \right)^{5/2} < \frac{1}{1956n^{5/2}}. \quad (33)$$

The excellent accuracy of the expansion Eq. (32) for I_n is apparent from Fig. 2(a).

To compute the Coulomb integral $f_0(z)$, we need, last but not least, to perform the summation according to Eq. (14). The result is given in Eq. (34), which we call the Chebyshev-Edgeworth projection of the Coulomb force,

$$f_0(z) = \frac{\sqrt{2\pi}}{\sigma} \frac{1}{z} \left(\text{Li}_{-(1/2)}(z) + \frac{\mu_4 - 3}{8} \text{Li}_{(1/2)}(z) \right.$$

$$\left. + \frac{75 - 90\mu_4 + 35\mu_4^2 - 8\mu_6}{384} \text{Li}_{(3/2)}(z) \right)$$

$$+ \Delta_{f_0}(z). \quad (34)$$

Based on Eq. (33) and on Eq. (36) we can evaluate an upper bound for the remainder $\Delta_{f_0}(z)$ in Eq. (34)

$$0 < \Delta_{f_0}(z) < \frac{1}{1956z} \text{Li}_{(3/2)}(z) \le (1/1956)\text{Li}_{3/2}(1)$$

$$< \frac{1}{1236}. \quad (35)$$

More details of the error estimation can be found in Appendices E–G. The function $\text{Li}_s(z)$ denotes Jonquière's polylogarithm [32], defined for all $|z| < 1$ and for all $s \in \mathbb{C}$ as

$$\text{Li}_s(z) = \sum_{n=1}^{\infty} \frac{z^n}{n^s}. \quad (36)$$

Note the relation with Riemann's ζ function [33] $\zeta(z)$ relevant to us,

$$\text{Li}_s(1) = \zeta(s). \quad (37)$$

Figure 2(b) shows that the Chebyshev-Edgeworth projection produces excellent results for the Coulomb integral Eq. (13). The underlying reason is that the Chebyshev-Edgeworth expansion maintains the exact singularity structure of the Coulomb integral. This does not hold true for the approach of Younis *et al.* [19].
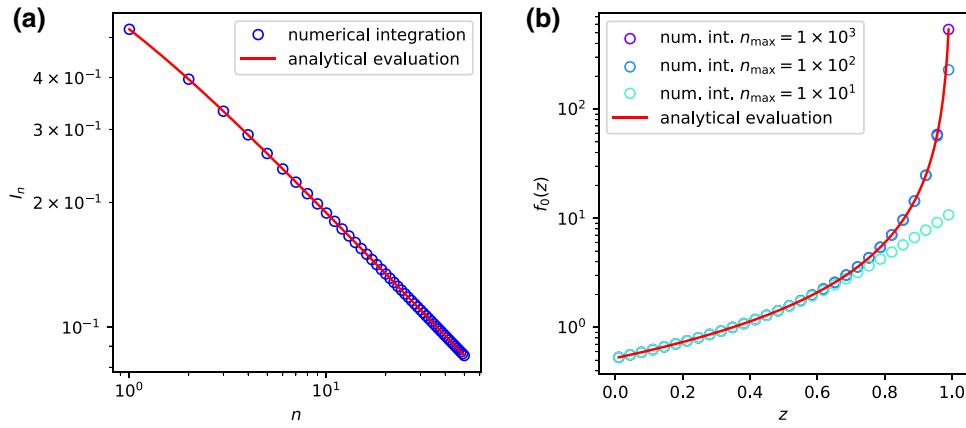
FIG. 2.　(a) Comparison of two methods to compute the integrals I_n according to Eq. (15). Open circles mark the results from direct numerical integration. The red line is the result of the Chebyshev-Edgeworth formula Eq. (32). (b) Comparison of two methods to compute the Coulomb integral $f_0(z)$ as defined by Eq. (13). Open circles mark the results from evaluating the sum Eq. (14) up to a certain maximum number of terms n_{max} by direct numerical integration. The red line is the Chebychev-Edgeworth projection Eq. (34) of the Coulomb force, neglecting the remainder $\Delta_{f_0}(z)$.

D. The singular structure of the Coulomb integral

The Chebyshev-Edgeworth projection formula Eq. (34) may actually appear a bit awkward, from a practitioners point of view. In the following we seek to improve this. The key information contained in Eq. (34) is how exactly to deal with the Coulomb force: The zero-mode approximation is a projection of the beam equation, Eq. (1), from the infinite-dimensional Hilbert space of all Euler-Bernoulli eigenmodes onto the one-dimensional subspace, spanned by the zero mode $\psi_0(z)$ only. *A priori*, it is far from obvious what this means for the Coulomb force. Note that this kind of question arises in any type of Galerkin procedure applied to Eq. (1). Equation (34) allows us to give the answer in the case of the zero-mode approximation, leading to a more practical version of our projection formula.

The contact singularity of the Coulomb force obviously causes a singularity of the Coulomb integral $f_0(z)$ at $z = 1$. The information about this singularity is entirely contained in the polylogarithms $\mathrm{Li}_{-(1/2)}(z)$ and $\mathrm{Li}_{+(1/2)}(z)$; all polylogarithms of larger index are regular,

$$\mathrm{Li}_{-(1/2)}(z) = \mathrm{Li}_{-(1/2)}(1) + \frac{\sqrt{\pi}}{2(1-z)^{3/2}}$$
$$- \frac{\sqrt{3\pi}}{8(1-z)^{1/2}} + O(1-z)^{1/2},$$
$$\mathrm{Li}_{1/2}(z) = \mathrm{Li}_{1/2}(1) + \frac{\sqrt{\pi}}{(1-z)^{1/2}} + O(1-z)^{1/2},$$
$$\mathrm{Li}_{n+\frac{1}{2}}(z) = \mathrm{Li}_{n+\frac{1}{2}}(1) + O(1-z)^{1/2}, \quad 0 < n \in \mathbb{N}.$$
$$(38)$$

This local analysis reveals that $f_0(z)$ as defined in Eq. (13) has the singular structure,

$$f_0(z) = \hat{f}_0(z) + O(1-z)^{1/2},$$
$$\hat{f}_0(z) = a + \frac{b}{(1-z)^{1/2}} + \frac{c}{(1-z)^{3/2}}. \qquad (39)$$

We now wish to find an algebraic approximation of the form $\hat{f}_0(z)$ to Eq. (34) that is as accurate as possible over the entire range $0 \le z \le 1$. This means we give up a little bit of the achieved accuracy at the singularity, in exchange for a global approximation, that pointwise has a relative error small enough for all practical purposes. To this end we demand that a, b, and c minimize the distance between $f_0(z)$ and its algebraic approximation $\hat{f}_0(z)$ with respect to a suitable norm in function space. The challenge here is the isolated singularity at $z = 1$. The associated lack of integrability can however be mended by introducing an apt non-negative weight function $r(z)$. The weight function should be selected such that it has a zero of sufficiently high degree compensating the singularity. Having said this, we choose the coefficients a, b, and c to minimize the functional

$$\mathcal{S}_r(a,b,c) = \int_0^1 r(z) \left(f_0(z) - \hat{f}_0(z) \right)^2 dz. \qquad (40)$$

A suitable $r(z)$ ensures the existence of this functional and of its Hessian as a positive definite matrix. Conceptually, an optimal weight function simultaneously minimizes the relative error. In practice, our simplistic choice, justified in arrears by Eq. (46), is

$$r(z) = (1-z)^3. \qquad (41)$$

With this weight function the Hessian is

$$\mathcal{H}ess(\mathcal{S}_r) = \begin{pmatrix} 1/4 & 2/7 & 2/5 \\ 2/7 & 1/3 & 1/2 \\ 2/5 & 1/2 & 1 \end{pmatrix}. \qquad (42)$$

Accordingly, there is a uniquely defined minimum, which is found solving for

$$\frac{\partial}{\partial a}\mathcal{S}_r(a,b,c) = 0 \Leftrightarrow H_a = \frac{a}{4} + \frac{2b}{7} + \frac{2c}{5},$$

$$\frac{\partial}{\partial b}\mathcal{S}_r(a,b,c) = 0 \Leftrightarrow H_b = \frac{2a}{7} + \frac{b}{3} + \frac{c}{2}, \qquad (43)$$

$$\frac{\partial}{\partial c}\mathcal{S}_r(a,b,c) = 0 \Leftrightarrow H_c = \frac{2a}{5} + \frac{b}{2} + c.$$

The constants H_a, H_b, and H_c are the integrals

$$H_a = \int_0^1 (1-z)^3 f_0(z)dz,$$

$$H_b = \int_0^1 (1-z)^{5/2} f_0(z)dz, \qquad (44)$$

$$H_c = \int_0^1 (1-z)^{3/2} f_0(z)dz.$$

Using suitable integer fractions we find the targeted algebraic expansion for $\hat{f}_0(z)$ to be,

$$\hat{f}_0(z) = \frac{1}{77} - \frac{1}{38(1-z)^{1/2}} + \frac{15}{28(1-z)^{3/2}}. \qquad (45)$$

The upper bound for the maximum relative error regarding this greatly simplified version of the Coulomb integral is easily computed analytically to be

$$\max_{0 \leq z \leq 1}\left(1 - \frac{\hat{f}_0(z)}{f_0(z)}\right) \leq \lim_{z \to 1}\left(1 - \frac{\hat{f}_0(z)}{f_0(z)}\right),$$

$$= 1 - \frac{15\sigma}{14\sqrt{2\pi}} < \frac{1}{494}. \qquad (46)$$

This is excellent for all practical purposes. In summary we show that the Coulomb singularity of Eq. (1) transforms into the quite different singularity given by the asymptotic expansion of Eq. (34), or for all practical purposes, by the global approximation Eq. (45), when projected onto the one-dimensional Hilbert subspace spanned by the Euler-Bernoulli zero mode. We believe that this result is of considerable practical relevance.
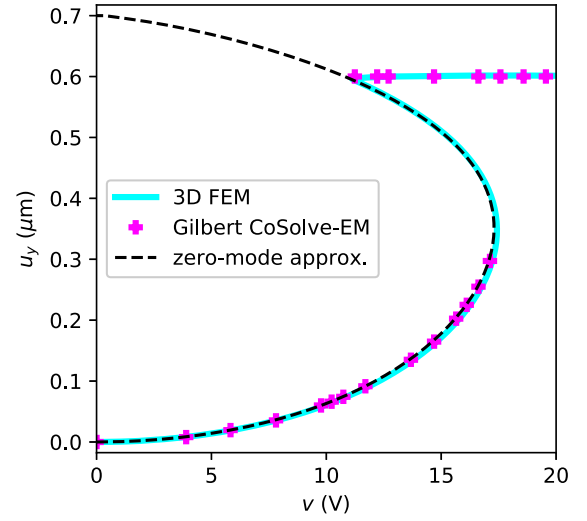

FIG. 3. Comparison of the deflection curve obtained from the zero-mode approximation Eq. (47) to the 3D simulation results from the literature (Gilbert CoSolve-EM [34] and 3D FEM [16]).

E. Synopsis of the zero-mode LPM

The zero-mode approximation

$$w(\xi, \tau) \approx z(\tau)\frac{\psi_0(\xi)}{\psi_0(0)},$$

developed in the previous section, leads upon careful treatment of the Coulomb singularity to the lumped-parameter model,

$$\frac{\partial^2}{\partial\tau^2}z + c\frac{\partial}{\partial\tau}z + k_0 z + \kappa z^3 = u^2\hat{f}_0(z),$$

$$\hat{f}_0(z) = \frac{1}{77} - \frac{1}{38(1-z)^{1/2}} + \frac{15}{28(1-z)^{3/2}},$$

$$\kappa = \alpha_1\left(\frac{\chi_0}{\psi_0(0)}\right)^2, \quad k_0 = \lambda_0 + N\chi_0, \qquad (47)$$

$$u = \psi_0(0)\sqrt{\alpha_2}v,$$

$$\alpha_1 = 6\left(\frac{g}{t}\right)^2, \quad \alpha_2 = \frac{6\epsilon l^4}{Et^3 g^3}.$$

Here l, t, and E denote length, thickness, and Young's modulus of the beam. g is the electrode gap. The definitions of $\psi_0(0)$ and χ_0 can be found in Eqs. (8), (9), and (11). For higher precision, Eq. (34) or any refinement thereof, can be used instead of Eq. (45). The bifurcation diagram, showing the static deflection of the beam center as a function of the drive voltage, is obtained as the set of all points in the (u, z) plane, solving the purely algebraic equation

$$\kappa z^3 + k_0 z = u^2\hat{f}_0(z). \qquad (48)$$

Equation (48) is best used by looking upon the voltage u as a function of the deflection, i.e., $u = u(z)$. The static pull-in
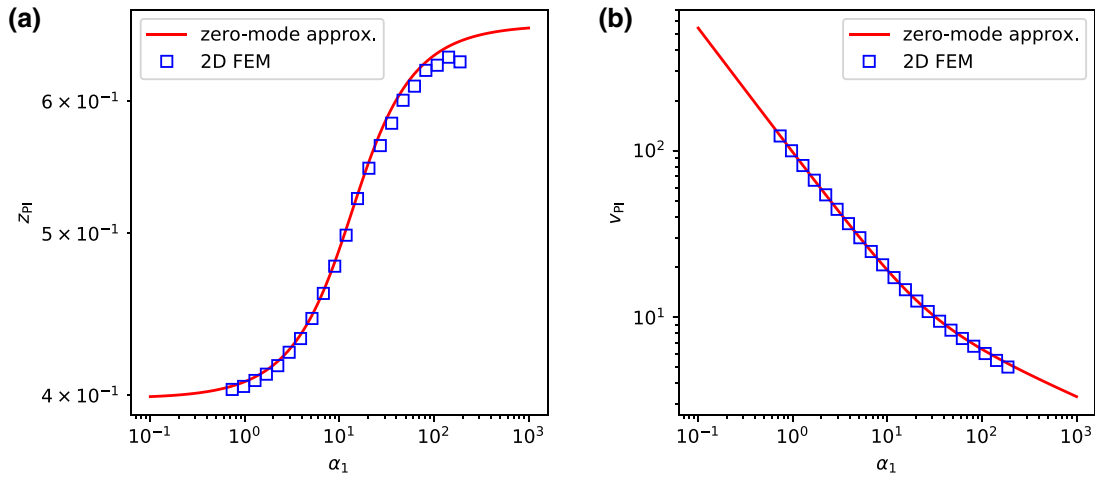
FIG. 4.   (a) The pull-in deflection z of a Coulomb actuated beam obtained by ANSYS (blue squares) and by zero-mode approximation Eq. (52) as a function of α_1 (solid red line). (b) The pull-in voltage of a Coulomb actuated beam simulated by ANSYS (blue squares) in comparison to simulations based on the zero-mode approximation Eq. (52) and Eq. (48) as a function of α_1 (solid red line).

deflection z_{PI} is reached at the critical point where

$$\frac{\partial u}{\partial z}(z_{PI}) = 0. \tag{49}$$

This condition is conveniently exploited by taking the inverse of the logarithmic derivative of Eq. (48). As shown in Eq. (51) below, within very small error margins, the inverse of the logarithmic derivative of the Coulomb integral is a linear function of the deflection amplitude z,

$$\left(\frac{\partial}{\partial z}\log(f_0(z))\right)^{-1} = \frac{64}{97} - \frac{44}{67}z - \Delta_{\log}(z). \tag{50}$$

The approximation Eq. (50) is obtained upon inserting Eq. (14) into the left-hand side of Eq. (50) and performing a Taylor expansion. The maximum error occurs at $z = 1$ where the left-hand side of Eq. (50) vanishes, due to the nature of its singularity as exhibited in Eq. (39). This puts a tight absolute bound on the remainder $\Delta_{\log}(z)$,

$$0 \leq \Delta_{\log}(z) < \frac{1}{325}. \tag{51}$$

It should be emphasized, that the derivation of Eq. (50) does not require using Eq. (45) or any other approximation discussed in this paper. The absolute upper bound of the remainder $\Delta_{\log}(z)$ is therefore not affected by any choice or error estimate made elsewhere. The highly effective approximation Eq. (50) leads to a simple algebraic equation for the practical evaluation of the pull-in deflection z_{PI},

$$\frac{\kappa z_{PI}^3 + k_0 z_{PI}}{3\kappa z_{PI}^2 + k_0} \approx \frac{64}{97} - \frac{44}{67}z_{PI}. \tag{52}$$

A first easy conclusion that can be drawn from Eq. (52) is that the pull-in deflection of a Coulomb actuated clamped-clamped Euler-Bernoulli beam varies within the limits

$$0.3982 \leq z_{PI} \leq 0.6664. \tag{53}$$

The lower bound of Eq. (53) is obtained as the limiting case of Eq. (52), where the stress stiffening (Duffing) coefficient κ vanishes. Likewise, the upper bound of Eq. (53) results from Eq. (52) in the case of an infinitely large κ. Within the realm of Euler-Bernoulli theory, these boundaries are independent of the shape of the beam cross section. While this fact certainly is known from numerical studies [16], it is derived here based on an analytical model.

Once we know z_{PI}, we can find the respective pull-in voltage u_{PI} using Eq. (48). The simple recipe presented in this section, requires little more than a spreadsheet or a pocket calculator to compute the pull-in data and the entire bifurcation diagram, with the astonishing numerical accuracy exhibited in Figs. 3–5.

F. LPM analysis of the beam used by Gilbert *et al.*

As a first application of our single degree of freedom LPM, we use the zero-mode approximation to compute the equilibria of the Coulomb actuated prismatic Euler-Bernoulli beam studied by Gilbert *et al.* [34]. For this exercise we apply the formulae compiled in Sec. III E. Gilbert *et al.* used the geometrical dimensions: beam length $l = 80\ \mu$m, beam width $w = 10\ \mu$m, beam thickness $t = 0.5\ \mu$m, electrostatic gap $g = 0.7\ \mu$m, and stop layer $s = 0.1\ \mu$m. For silicon, Gilbert *et al.* used an isotropic stiffness with a Young's modulus of $E = 169$ GPa and a Poisson ratio of $\nu = 0.25$. The zero-mode results are compared to the results of Gilbert *et al.* [34] and to the
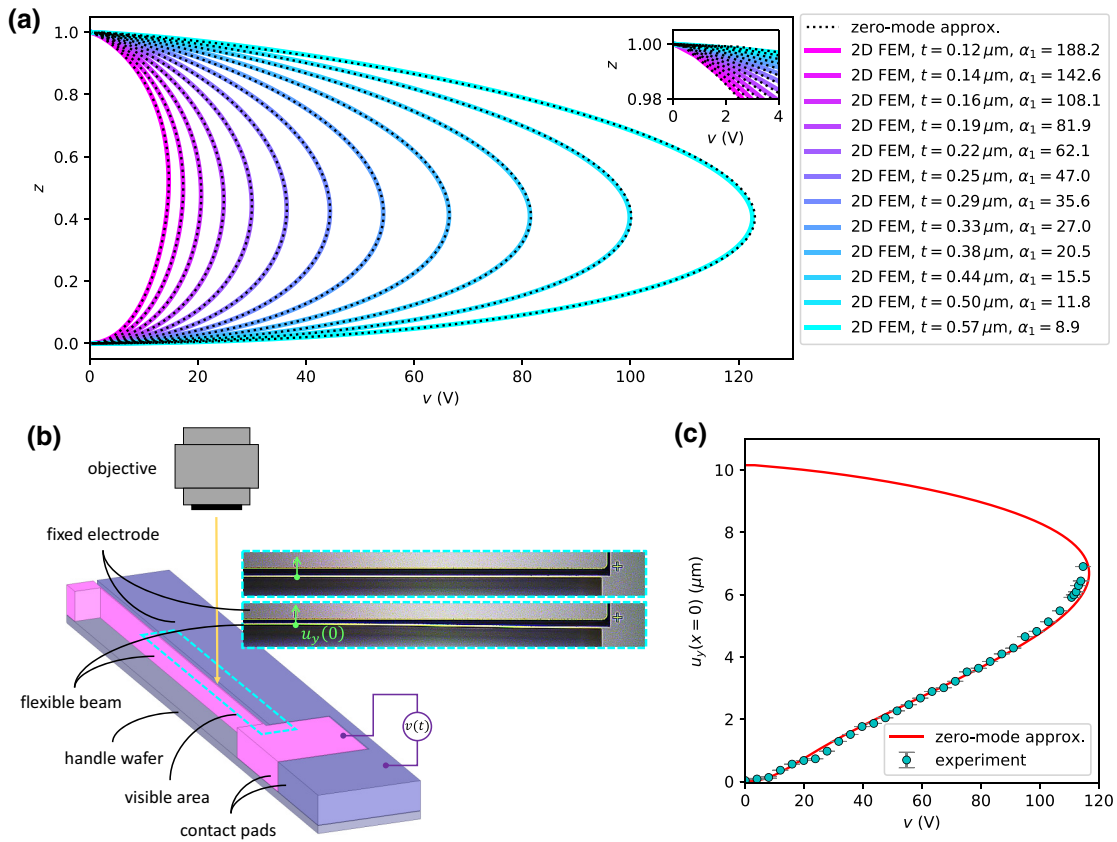
FIG. 5. (a) The equilibria of a Coulomb actuated beam as obtained by ANSYS (colored solid lines) and by the zero-mode approximation Eq. (47) (dotted black lines) for $l = 80$ μm, $g = 0.7$ μm and various thicknesses t. (b) The experimental setup and example frames used for the deflection measurement. (c) Measured equilibria of a Coulomb actuated beam (filled cyan circles) compared to the zero-mode approximation (solid red line) according to Eq. (47) as a function of the voltage.

three-dimensional (3D) ANSYS simulation by Melnikov *et al.* [16] in Fig. 3. Obviously there is a very good agreement between our zero-mode approximation based on the Chebyshev-Edgeworth expansion and the results of Gilbert *et al.* [34] and Melnikov *et al.* [16] The deflection profile, the pull-in voltage, and the pull-out voltage can be reliably determined using our method.

G. Comparison with the numerical and experimental results of Melnikov *et al.*

Melnikov *et al.* [16] used a continuation method to extend the reach of FEM simulations to the entire bifurcation diagram of Coulomb actuated prismatic clamped-clamped Euler-Bernoulli beams, including all stable and unstable equilibria. They calculated the respective bifurcation diagrams and pull-in voltages for microbeams with a length of $l = 80$ μm, a thickness range between $t = 0.12$ μm and $t = 2$ μm, and an electrode gap of $g = 0.7$ μm.

Figure 4 shows the pull-in deflection and the pull-in voltage, respectively. These graphs demonstrate the excellent match of the zero-mode approximation and the

FEM results. Additionally, Fig. 5 reveals an almost perfect agreement between FEM results and the zero-mode approximation, regarding the entire deflection profiles, including their unstable branches. We note that the solution close to the contact singularity at $z = 1$ is correctly reproduced using a single mode.

Melnikov *et al.* [16] scrutinized their findings by running a MEMS experiment. The basic experimental setup is shown in Fig. 5(b). A clamped-clamped MEMS microbeam of length $l = 1000$ μm, width $w = 75$ μm, and with a measured thickness of $t = 2.47$ μm is manufactured on a bonded silicon on insulator (BSOI) wafer, to perform in-plane movements. The beam is Coulomb actuated by a planar electrode positioned in front of the beam at a distance of $g = 10.15$ μm (fitted electrode gap). The beam movement is enabled by removing the oxide layer underneath the beam by etching with hydrofloric acid. The details of the experiment can be found in Melnikov *et al.* [16]. Furthermore, a small compression stress of 2.6 MPa is used for the zero-mode approximation. The presence of such stress is consistent with previous observations by Younis *et al.* [19] and Melnikov *et al.* [16], while it is likely to be residual stress from manufacturing. The experimental

findings are well reproduced by the simple LPM developed in this paper, as can be seen in Fig. 5(c).

In summary we find that the zero-mode approximation gives rise to a simple LPM with a single degree of freedom, well suited to quantitatively describe all stable and unstable equilibria of clamped-clamped Coulomb actuated prismatic Euler-Bernoulli beams.

IV. DISCUSSION

Spitz *et al.* [35] observed that the performance of a fairly complex MEMS μSpeaker can be successfully modeled by a heuristic single degree of freedom lumped-parameter model. Motivated by this research, Melnikov *et al.* [16] revisited the analysis of the bending profile of a Coulomb-activated prismatic microbeam, clamped at both ends: the study clearly confirms that the bending profile stays almost identical to the shape of the Euler-Bernoulli zero mode, independent of the load. This is true for the entire applicable voltage range within a very small error margin. The observations of Melnikov *et al.* [16] allowed us here to develop the single degree of freedom lumped-parameter model, Eq. (47), capable of accurately describing all stable and unstable equilibria of this highly nonlinear electromechanical system. The existence of an accurate single degree of freedom LPM is not reported in the literature. In fact the literature claims the need for higher modes [22].

The zero-mode approximation requires a method correctly projecting the Coulomb force onto the one-dimensional Hilbert subspace, spanned by the Euler-Bernoulli zero-mode Eq. (8). Such a projection is a global task in function space, that cannot be performed using local techniques, such as a plain Taylor expansion. The ideas of Chebyshev and Edgeworth, underlying the original proof of the celebrated central limit theorem, furnish us here with the required means. As a result we obtain the analytical projection formula Eq. (34) for the Coulomb force. This formula allows us to extract the exact form of the contact singularity of the projected Coulomb force. Based on this knowledge, a global analysis of the Coulomb integral can be performed, leading to the handy algebraic expression Eq. (45). This completes the derivation of our highly accurate and simple to use lumped-parameter model. A utilization of the Chebyshev-Edgeworth method to solve a nonlinear differential equation has not been reported in the literature before.

The results presented above now allow the efficient computation of the detailed frequency response and harmonic distortion of electromechanic MEMS transducers, with little computational effort. For practical applications, such dynamic computations are enabled by the large spectral distance of the Euler-Bernoulli zero mode from higher Euler-Bernoulli modes, see Melnikov *et al.* [16]. We note that the approach is applicable not only to clamped-clamped microbeams, but also to other conditions such as

pinned-pinned or clamped-free. In such a case, Eq. (8) can stay the same while Eq. (9) changes, resulting in an alternative β and alternative coefficient in Eq. (8). Certainly, time-dependent FEM simulations will always allow substantially more complex MEMS actuator geometries to be handled. However, the process of basic actuator design, as well as the circuit simulation of complex systems embracing MEMS actuators, see Monsalve *et al.* [36], greatly benefit from the availability of powerful LPM models.

We present the use of Chebyshev-Edgeworth methods in this paper to model a very particular situation. While our focus on a simple case may help to understand the basic principle, it probably is misleading at the same time. Chebyshev-Edgeworth methods apply to far more general situations and allow for a broad range of applications. These include different boundary conditions, nonprismatic beams, the modeling of squeeze film damping, the computation of electric fringe field corrections and of contact forces to name a few. In addition, research on zero dispersion in oscillatory systems [37] might benefit from our results. For example, the results of Huang *et al.* [38] on the trampoline resonator can be applied to a much broader class of resonators, including elastic resonators with stress stiffening. From a more general point of view, the Chebyshev-Edgeworth approach could also be used to find a closed form of the frequency-to-energy dependence in devices such as superconducting quantum interference devices [37]. For the sake of clarity, we defer sharing the details of such generalizations to forthcoming publications.

V. CONCLUSION

All stable and unstable equilibrium states of Coulomb actuated prismatic clamped-clamped Euler-Bernoulli beams can be accurately computed by the user-friendly Eq. (47). This LPM features only one degree of freedom, i.e., the amplitude of the Euler-Bernoulli zero mode. The difference of our results to previous findings of other groups are easily understood in terms of the advanced methods outlined above to adequately treat the Coulomb singularity. We apply a Chebyshev-Edgeworth expansion, originating from probability theory, for the solution of nonlinear partial differential equations. In addition, we believe that this approach is not limited to nonlinear beam mechanics and opens a way to evaluate certain integrals with a kernel close to a singularity.

APPENDIX A: THE EULER-BERNOULLI BEAM EQUATION FOR PRISMATIC BEAMS

A prismatic Coulomb-actuated microbeam according to Fig. 6(b) can be modeled according to the following

equation [24]:

$$\frac{\partial^2 w}{\partial \tau^2} + c\frac{\partial w}{\partial \tau} + \frac{\partial^4 w}{\partial \xi^4} = (\gamma[w] + N)\frac{\partial^2 w}{\partial \xi^2} + \alpha_2 \frac{v(\tau)^2}{(1-w)^2},$$

(A1)

where ξ, τ, c, and $w(\xi, \tau)$ are dimensionless quantities, denoting the coordinate along the beam, the time, the damping, and the lateral displacement. N is a dimensionless external tensile axial force and $\gamma[w]$ is the stress stiffening, which actually is a nonlocal functional of the deflection $w(\xi, \tau)$,

$$\gamma[w] = \alpha_1 \int_{-(1/2)}^{+(1/2)} \left(\frac{\partial w}{\partial \zeta}\right)^2 d\zeta.$$

(A2)

α_1 and α_2 are geometry-dependent parameters, and $v(\tau)$ is the drive voltage. The dimensionless quantities are defined as follows:

$$\xi = \frac{x}{l},$$

(A3)

with x being the coordinate along the beam and l the length of the beam in absolute terms:

$$w = \frac{u}{g},$$

(A4)

u being the displacement in the direction of the fixed electrode and g the electrode gap at zero deflection in absolute terms:

$$\alpha_1 = 6\left(\frac{g}{t}\right)^2,$$

(A5)

t being the beam thickness in absolute terms:

$$\alpha_2 = \frac{6\epsilon l^4}{Et^3 g^3}$$

(A6)

and ϵ is the dielectric constant of the gap medium and E is Young's modulus of the beam [24].

For a clamped-clamped beam we have the boundary conditions

$$w\left(-\frac{1}{2}, \tau\right) = w\left(+\frac{1}{2}, \tau\right) = 0,$$
$$\frac{\partial w}{\partial \xi}\left(-\frac{1}{2}, \tau\right) = \frac{\partial w}{\partial \xi}\left(+\frac{1}{2}, \tau\right) = 0.$$

(A7)

In this paper we consider the static deflections only: all time derivatives are set to zero. For small deflections the effect of the stress stiffening can be neglected. Note that upon reducing the drive voltage v to zero, a Coulomb-actuated beam, originally in a stable state will, return to zero deflection. This means that the effect of the Coulomb force approaches that of a constant load of magnitude $\alpha_2 v^2$. The same situation occurs with thicker beams beyond the scope of Euler-Bernoulli theory.

TABLE I. Values of β_{2n}. Comparison between numerically calculated and approximated values for β_{2n}.

$2n$	β_{2n}	$[2n + (3/2)]\pi$
0	4.73004	4.71239
2	10.9956	10.9956
4	17.2788	17.2788
6	23.5619	23.5619

APPENDIX B: SYMMETRIC EULER-BERNOULLI EIGENMODES

For a prismatic beam, clamped at both ends, the Euler-Bernoulli eigenmodes are defined by the eigenvalue equation

$$\frac{\partial^4}{\partial \xi^4}\psi_n(\xi) = \lambda_n \psi_n(\xi),$$

(B1)

subject to the boundary conditions Eq. (A7). The eigensystem for even indices, λ_{2n} and $\psi_{2n}(\xi)$, are given by

$$\psi_{2n}(\xi) = \frac{\cosh(\beta_{2n}\xi)}{\cosh(\beta_{2n}/2)} - \frac{\cos(\beta_{2n}\xi)}{\cos(\beta_{2n}/2)},$$

(B2)

$$\lambda_{2n} = \beta_{2n}^4,$$

(B3)

$$0 < \lambda_0 < \lambda_2 < \cdots < \lambda_{2n} < \cdots,$$

where the β_{2n} are the zeros of

$$0 = \tanh\left(\frac{\beta_{2n}}{2}\right) + \tan\left(\frac{\beta_{2n}}{2}\right),$$

(B4)

which can be approximated using

$$z_{2n} = \left(2n + \frac{3}{2}\right)\pi,$$

$$\beta_{2n} = z_{2n} + 2\exp[-z_{2n}] + O[\exp[-z_{2n}]]^2.$$

(B5)

Table I illustrates numerically determined β_{2n} from Eq. (B4) in comparison to the approximation using only the first term in Eq. (B5).

It is readily verified that the function in Eq. (B2) satisfies Eq. (B1) and the boundary conditions in Eq. (A7). Note that the eigenmodes as defined above are orthonormal,

$$\int_{-(1/2)}^{+(1/2)} \psi_{2n}(\xi)\psi_{2m}(\xi)d\xi = \begin{cases} 1, & \text{if } n = m \\ 0, & \text{if } n \neq m. \end{cases}$$

(B6)

Moreover, the even eigenmodes form a complete orthonomal base of the Hilbert space of symmetric square integrable functions over the interval $\left[-\frac{1}{2}, +\frac{1}{2}\right]$. This means
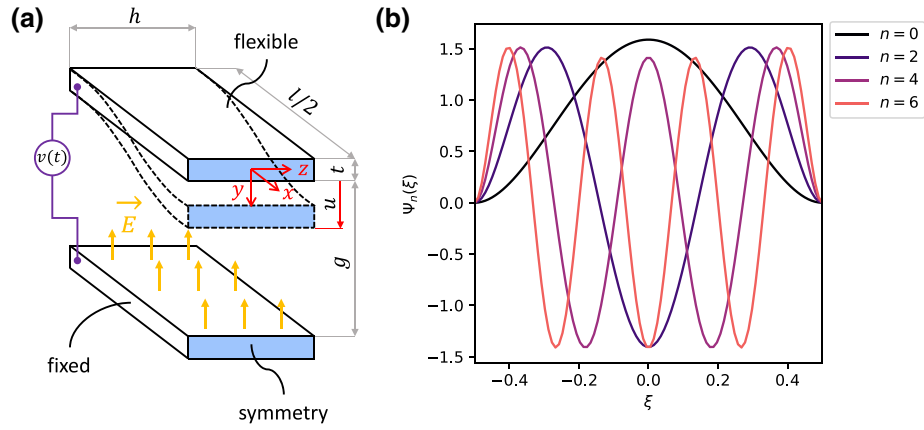
FIG. 6. (a) Schematic of a prismatic Coulomb-actuated microbeam in undeflected (solid lines) and deflected (dashed lines) states including characteristic dimensions and the coordinate system. (b) The first four symmetric normal-mode shapes for an Euler-Bernoulli beam in CC condition. (Adapted from Ref. [16].)

that we can expand any symmetric deflection profile $w(\xi)$ in terms of these eigenmodes

$$w(\xi) = \sum_{n=0}^{\infty} \hat{w}_{2n} \psi_{2n}(\xi), \tag{B7}$$

where we have due to orthonormality

$$\hat{w}_{2n} = \int_{-(1/2)}^{+(1/2)} w(\xi) \psi_{2n}(\xi) d\xi. \tag{B8}$$

APPENDIX C: COMPUTING THE MOMENTS μ_{2n}

First we use the explicit form of the zero mode to compute σ,

$$\sigma^2 = \beta_0^2 \frac{\cos(\beta_0/2) + \cosh(\beta_0/2)}{\cos(\beta_0/2) - \cosh(\beta_0/2)} \approx 17.1256. \tag{C1}$$

The other moments are obtained from Eq. (28) by repeated differentiation of the eigenvalue equation at $\xi = 0$,

$$\psi_0^{(4k+r)}(0) = \lambda_0^k \psi_0^{(r)}(0), \\ k \in \mathbf{N}, \ r \in \{0, 1, 2, 3\}. \tag{C2}$$

Inserting Eqs. (C2), (C1), and (B3) into Eqs. (28) yields Eq. (29). For our purposes it is sufficient to compute μ_4 and μ_6,

$$\mu_4 = \mu_6 = \frac{\lambda_0}{\sigma^4} \approx 1.70674. \tag{C3}$$

APPENDIX D: COMPUTING THE EDGEWORTH POLYNOMIALS $c_1(\xi)$ AND $c_2(\xi)$

First we cast Eq. (16) into the form

$$\Phi_n(\xi) = \frac{1}{\sqrt{2\pi}} \left[\sqrt{2\pi} \phi_1 \left(\frac{\xi}{\sqrt{n}} \right) \right]^n. \tag{D1}$$

Then we insert the expansion Eqs. (27) into (D1) and use the following formula for $k_{\max} \geq 3$:

$$e^{-a_1} \left(1 + \sum_{k=1}^{k_{\max}} \frac{a_k}{n^k} \right)^n = 1 + \frac{2a_2 - a_1^2}{2n} + \frac{1}{2} \left(\frac{2a_2 - a_1^2}{2n} \right)^2 \\ + \frac{a_1^3 - 3a_2 a_1 + 3a_3}{3n^2} + O\left(\frac{1}{n} \right)^3. \tag{D2}$$

Upon collecting the coefficients of the respective power of $1/n$, we obtain the targeted polynomials $c_1(\xi)$ and $c_2(\xi)$.

APPENDIX E: ESTIMATING THE REMAINDER Δ_n

As can be inferred from Fig. 7(b), the maximum error Δ_n occurs at $n = 2$. The solid red line of Fig. 7(b) depicts the graph of the function

$$\Delta_n \leq \Delta_2 \left(\frac{2}{n} \right)^{5/2}, \tag{E1}$$

which obviously is an upper bound for the error Δ_n. So the task is computing Δ_2. According to Eq. (15) and the
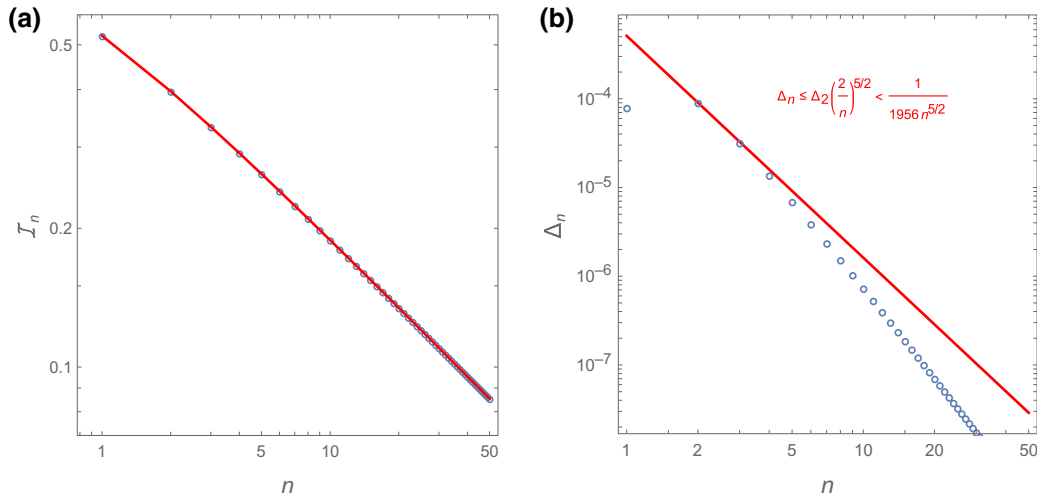
FIG. 7. Assessing the quality of the Chebyshev-Edgeworth expansion of the integrals I_n according to Eq. (32). (a) The integrals I_n evaluated by numerical integration (blue circles) and by means of the Chebyshev-Edgeworth expansion (solid red line) as a function of the index n. (b) The remainder Δ_n computed as the difference of the integrals I_n evaluated by numerical integration and the corresponding values obtained by the Chebyshev-Edgeworth expansion (blue circles), compared to the upper bound according to Eq. (33) (solid red line).

orthonormality Eq. (B6) we get

$$I_2 = \frac{1}{\psi_0(0)^2}. \tag{E2}$$

With this, Eq. (32) leads to

$$\Delta_2 = \frac{1}{\psi_0(0)^2} - \frac{\sqrt{\pi}}{512\sigma}\left(411 + 2\mu_4 + 9\mu_4^2\right). \tag{E3}$$

APPENDIX F: ESTIMATING THE REMAINDER $\Delta_{f_0}(z)$ OF THE CHEBYSHEV-EDGEWORTH PROJECTION

From Eqs. (14) and (32) we get

$$\Delta_{f_0}(z) = \sum_{n=1}^{\infty} n\Delta_n z^{n-1}. \tag{F1}$$

Using the estimate Eq. (33) and the definition Eq. (35) we conclude

$$0 \le \Delta_{f_0}(z) \le 2^{5/2}\Delta_2 \sum_{n=1}^{\infty} \frac{z^{n-1}}{n^{3/2}} = \frac{2^{5/2}\Delta_2}{z}Li_{3/2}(z). \tag{F2}$$

To find an absolute upper limit for $\Delta_{f_0}(z)$, we observe that according to Fig. 8(b),

$$\max_{0 \le z \le 1} \Delta_{f_0}(z) = \Delta_{f_0}(1). \tag{F3}$$

An upper bound for $\Delta_{f_0}(1)$ is easily from our estimate Eq. (F2),

$$\Delta_{f_0}(1) \le 2^{5/2}\Delta_2 Li_{3/2}(1) = 2^{5/2}\Delta_2\zeta\left(\frac{3}{2}\right). \tag{F4}$$

APPENDIX G: ESTIMATING THE ERROR OF $\hat{f}_0(z)$

We define the relative error $\Delta_r(z)$ the algebraic approximation $\hat{f}_0(z)$ as

$$\Delta_r(z) = \left(1 - \frac{\hat{f}_0(z)}{f_0(z)}\right). \tag{G1}$$

Figure 9(b) shows that this error reaches its absolute maximum at $z = 1$,

$$\max_{0 \le z \le 1} \Delta_r(z) = \lim_{z \to 1} \Delta_r(z). \tag{G2}$$

The challenge computing this limit is due to the fact that both, $f_0(z)$ and $\hat{f}_0(z)$ become singular at this point. This can be mended by multiplying each of these functions by a factor of $(1 - z)^{3/2}$,

$$\lim_{z \to 1} \Delta_r(z) = \lim_{z \to 1} \left(1 - \frac{(1-z)^{3/2}\hat{f}_0(z)}{(1-z)^{3/2}f_0(z)}\right). \tag{G3}$$

The limit for $\hat{f}_0(z)$ is easily calculated from the leading singularity in Eq. (45)

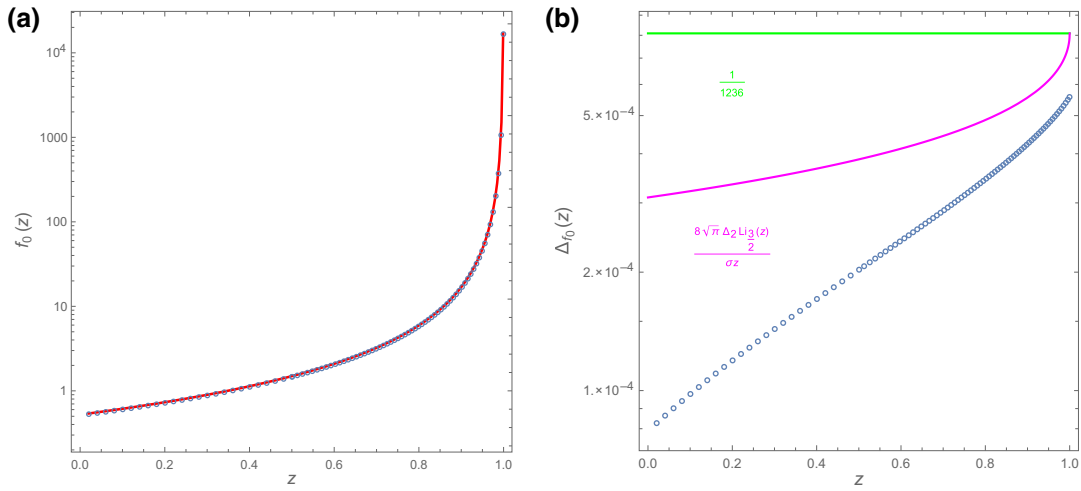$$\lim_{z \to 1}(1-z)^{3/2}\hat{f}_0(z) = \frac{15}{28}. \tag{G4}$$

FIG. 8. Assessing the quality of the Chebyshev-Edgeworth projection Eq. (34) of the Coulomb force. (a) The Coulomb integral $f_0(z)$ evaluated by numerical integration (blue circles) and by means of the projection formula (solid red line) as a function of z. (b) The remainder $\Delta_{f_0}(z)$ computed as the difference of the Coulomb integral $f_0(z)$ evaluated by numerical integration and the corresponding values obtained by the projection formula (blue circles), compared to the upper bounds according to Eq. (37) (solid magenta and green lines).

Likewise, we use Eq. (34) and the asymptotic expansion Eq. (38) to conclude

$$\lim_{z \to 1}(1-z)^{3/2}f_0(z) = \frac{\sqrt{2\pi}}{\sigma}\frac{\sqrt{\pi}}{2}. \quad \text{(G5)}$$

Finally, we insert Eq. (G4) and (G5) into the left-hand side of Eq. (G3) obtaining

$$\Delta_r(z) \le \lim_{z \to 1}\Delta_r(z) = 1 - \frac{15\sigma}{14\sqrt{2\pi}} \le \frac{1}{494}. \quad \text{(G6)}$$

APPENDIX H: LOGARITHMIC DERIVATIVE OF THE COULOMB INTEGRAL

In this section we derive Eq. (50). Figure 10(a) reveals that the inverse of the logarithmic derivative of the Coulomb integral is almost exactly a linear function of z. The tricky part to understand this, is showing that the inverse of the logarithmic derivative has a zero at $z = 1$, despite the singularity of $f_0(z)$ at this point,

$$\lim_{z \to 1}\left(\frac{\partial}{\partial z}\log(f_0(z))\right)^{-1} = 0. \quad \text{(H1)}$$
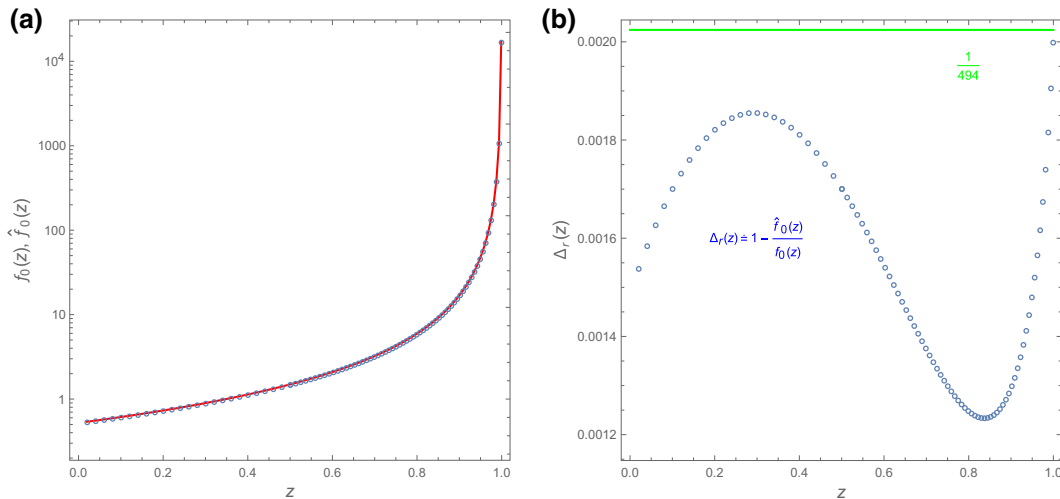

FIG. 9. Assessing the quality of the algebraic approximation $\hat{f}_0(z)$ to the Coulomb integral according to Eq. (45). (a) The algebraic approximation $\hat{f}_0(z)$ (solid red line) compared to the Coulomb integral $f_0(z)$ evaluated by numerical integration (blue circles) as a function of z. (b) The relative error $\Delta_r(z)$ computed as the relative deviation of the algebraic approximation $\hat{f}_0(z)$ from the numerically evaluated Coulomb integral $f_0(z)$ (blue circles). The upper bound according to Eq. (46) is also shown (solid green line).
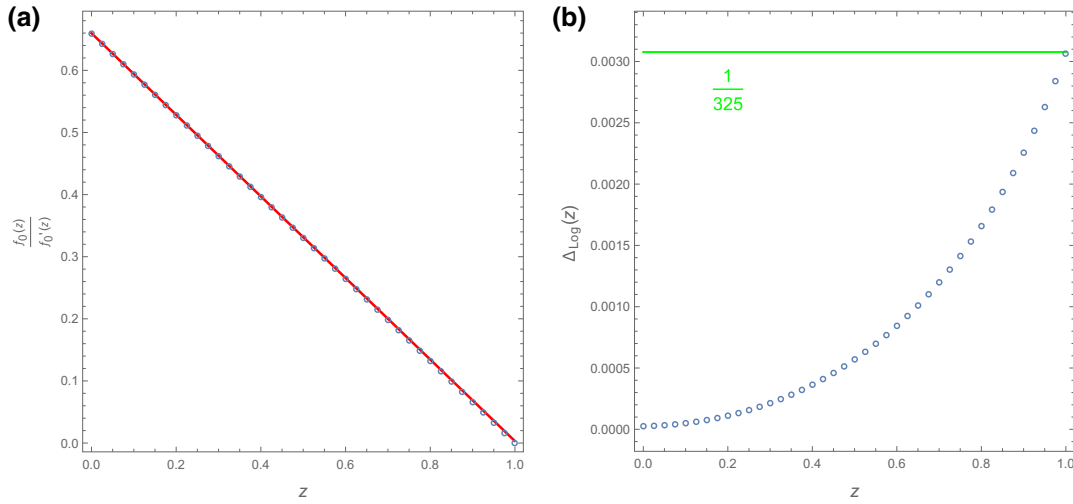
(a)

(b)

FIG. 10.   Assessing the quality of the linear approximation to the inverse of the logarithmic derivative of the Coulomb integral $f_0(z)$ according to Eq. (50). (a) The numerically evaluated inverse of the logarithmic derivative of the Coulomb integral $f_0(z)$ (blue circles) versus the linear approximation (solid red line) as a function of z. (b) The absolute deviation $\Delta_{\log}(z)$ of the linear approximation from the numerically evaluated inverse of the logarithmic (blue circles) and the upper error limit according to Eq. (51) (solid green line).

Thanks to Eq. (39) we know the exact nature of this singularity. Therefore, we can conclude

$$\lim_{z \to 1} \left(\frac{\partial}{\partial z} \log(f_0(z)) \right)^{-1} = \lim_{z \to 1} \left(\frac{\partial}{\partial z} \log(\frac{1}{(1-z)^{3/2}}) \right)^{-1}$$

$$= -\frac{2}{3} \lim_{z \to 1} \left(\frac{\partial}{\partial z} \log(1-z) \right)^{-1}$$

$$= 0. \qquad (H2)$$

In view of this, Eq. (50) proves that $\Delta_{\log}(1)$ has a finite value. Next we use the expansion Eq. (14) to evaluate

$$\left(\frac{\partial}{\partial z} \log(f_0(z)) \right)^{-1} = \frac{I_1 + 2I_2 z + O[z]^2}{2I_2 + 6I_3 z + O[z]^2}$$

$$= \frac{I_1}{2I_2} + \left(1 - \frac{3I_1 I_3}{2I_2^2} \right) z + \Delta_{\log}(z).$$

$$(H3)$$

Figure 10(b) finally shows that the remainder $\Delta_{\log}(z)$ is strictly positive and reaches its maximum at the singularity of the Coulomb integral $f_0(z)$,

$$0 < \Delta_{\log}(z) \leq \Delta_{\log}(1). \qquad (H4)$$

So the upper bound for $\Delta_{\log}(z)$ is easily calculated by applying Eqs. (H1) to (H3), i.e.,

$$0 = \frac{I_1}{2I_2} + \left(1 - \frac{3I_1 I_3}{2I_2^2} \right) + \Delta_{\log}(1). \qquad (H5)$$

[1] S. D. Senturia, *Microsystem Design* (Kluwer Academic Publishers, Boston, MA, 2002).

[2] C. T. Leondes, *MEMS/NEMS: Handbook Techniques and Applications* (Springer Science+Business Media Inc, Boston, MA, 2006).

[3] T.-R. Hsu, *MEMS and Microsystems: Design, Manufacture, and Nanoscale Engineering* (Wiley, Hoboken, NJ, 2008), 2nd ed.

[4] S. S. Saliterman, *Fundamentals of BioMEMS and Medical Microdevices*, SPIE Press Monograph Series (SPIE Press, Bellingham, WA, 2006). Vol. 153.

[5] S. Lucyszyn, Review of radio frequency microelectromechanical systems technology, IEE Proc.—Sci. Meas. Technol. **151**, 93 (2004).

[6] S. Li, L. D. Xu, and S. Zhao, 5G Internet of Things: A survey, J. Ind. Inf. Integr. **10**, 1 (2018).

[7] A. Coppa, E. Cianci, V. Foglietti, G. Caliano, and M. Pappalardo, Building CMUTs for imaging applications from top to bottom, Microelectron. Eng. **84**, 1312 (2007).

[8] S. Finkbeiner, in *2013 Proceedings of the ESSCIRC (ESSCIRC)* (IEEE, Bucharest, Romania, 2013), p. 9.

[9] X. Zou, P. Thiruvenkatanathan, and A. A. Seshia, A seismic-grade resonant MEMS accelerometer, J. Microelectromech. Syst. **23**, 768 (2014).

[10] T. Verdot, E. Redon, K. Ege, J. Czarny, C. Guianvarc'h, and J.-L. Guyader, Microphone with planar nano-gauge detection: Fluid-structure coupling including thermoviscous effects, Acta Acust. United Acust. **102**, 517 (2016).

[11] I. Shahosseini, E. Lefeuvre, J. Moulin, E. Martincic, M. Woytasik, and G. Lemarquand, Optimization and microfabrication of high performance silicon-based MEMS microspeaker, IEEE Sens. J. **13**, 273 (2013).

[12] B. Kaiser, S. Langa, L. Ehrig, M. Stolz, H. Schenk, H. Conrad, H. Schenk, K. Schimmanz, and D. Schuffenhauer,

Concept and proof for an all-silicon MEMS micro speaker utilizing air chambers, Microsyst. Nanoeng. **5,** 1 (2019).

[13] J.-H. Kim, N. D. Thang, and T.-S. Kim, in *IEEE International Symposium on Industrial Electronics, 2009* (IEEE, Piscataway, NJ, 2009), p. 1013.

[14] A. P. Bianzino, C. Chaudet, D. Rossi, and J.-L. Rougier, A survey of green networking research. ArXiv:1010.3880.

[15] T. Worthington, *ICT Sustainability: Assessment and Strategies for a Low Carbon Future* (LULU COM, 2017).

[16] A. Melnikov, H. A. G. Schenk, J. M. Monsalve, F. Wall, M. Stolz, A. Mrosk, S. Langa, and B. Kaiser, Coulomb-actuated microbeams revisited: Experimental and numerical modal decomposition of the saddle-node bifurcation, Microsyst. Nanoeng. **7,** 41 (2021).

[17] R. Lifshitz and M. C. Cross, in *Reviews of Nonlinear Dynamics and Complexity*, edited by H. G. Schuster (Wiley-VCH and John Wiley Distributor, Weinheim, Chichester, 2008), p. 1.

[18] A. N. Cleland, *Foundations of Nanomechanics: From Solid-State Theory to Device Applications*, Springer eBook Collection (Springer, Berlin and Heidelberg, 2003).

[19] M. I. Younis, E. M. Abdel-Rahman, and A. Nayfeh, A reduced-order model for electrically actuated microbeam-based MEMS, J. Microelectromech. Syst. **12,** 672 (2003).

[20] M. Younis, E. Abdel-Rahman, and A. Nayfeh, in *Structures, Structural Dynamics, and Materials and Co-located Conferences* (American Institute of Aeronautics and Astronautics, Denver, Colorado, 2002).

[21] Eihab M. Abdel-Rahman, Mohammad I. Younis, and Ali H. Nayfeh, Characterization of the mechanical behavior of an electrically actuated microbeam, J. Micromech. Microeng. **12,** 759 (2002).

[22] M. I. Younis and A. H. Nayfeh, A study of the nonlinear response of a resonant microbeam to an electric actuation, Nonlinear Dyn. **31,** 91 (2003).

[23] A. H. Nayfeh, M. I. Younis, and E. M. Abdel-Rahman, Reduced-order models for MEMS applications, Nonlinear Dyn. **41,** 211 (2005).

[24] A. H. Nayfeh, M. I. Younis, and E. M. Abdel-Rahman, Dynamic pull-in phenomenon in MEMS resonators, Nonlinear Dyn. **48,** 153 (2007).

[25] M. I. Younis, *MEMS Linear and Nonlinear Statics and Dynamics*, Microsystems (Springer Science+Business Media LLC, Boston, MA, 2011), Vol. 20.

[26] P. Tchebycheff, Sur deux théorèmes relatifs aux probabilités, Acta Mathematica **14,** 305 (1890).

[27] F. Y. Edgeworth, The law of error, Camb. Philos. Soc. **36,** 33 (1905).

[28] S. Lang, *Complex Analysis*, Springer eBook Collection Mathematics and Statistics (Springer, New York, NY, 1999), Vol. 103, 4th ed.

[29] O. Forster, *Analysis 3: Maß- und Integrationstheorie, Integralsätze im IRn und Anwendungen*, Aufbaukurs Mathematik (Springer Spektrum, Wiesbaden, 2017), 8th ed.

[30] D. L. Wallace, Asymptotic approximations to distributions, Ann. Math. Stat. **29,** 635 (1958).

[31] K. Königsberger, *Analysis 1*, Springer-Lehrbuch (Springer Berlin Heidelberg, Berlin, Heidelberg, 2001).

[32] A. Jonquière, Note sur la série $\sum_{(n=1)}^{(n=\infty)} (x^n)/(n^s)$, Bull. Soc. Math. France **17,** 142 (1889).

[33] B. Riemann, Über die Anzahl der Primzahlen unter einer gegebenen Grösse, Monatsber. Königl. Preuss. Akad. Wiss. Berlin, 671 (1859).

[34] J. R. Gilbert, G. K. Ananthasuresh, and S. D. Senturia, in *Proceedings/IEEE the Ninth Annual International Workshop on Micro Electro Mechanical Systems [MEMS]* (IEEE Service Center, Piscataway, NJ, 1996), p. 127.

[35] B. Spitz, F. Wall, H. Schenk, A. Melnikov, L. Ehrig, S. Langa, M. Stolz, B. Kaiser, H. Conrad, H. Schenk, and W. Pufe, Audio-Transducer for In-Ear-Applications based on CMOS compatible electrostatic actuators, MikroSystemTechnik Kongress Proceedings (2019), https://ieeexplore.ieee.org/abstract/document/9012783.

[36] J. M. Monsalve, A. Melnikov, B. Kaiser, D. Schuffenhauer, M. Stolz, L. Ehrig, H. A. G. Schenk, H. Conrad, and H. Schenk, Large-signal equivalent-circuit model of asymmetric electrostatic transducers, IEEE/ASME Trans. Mechatron., 1 (2021).

[37] S. M. Soskin, R. Mannella, and P. McClintock, Zero-dispersion phenomena in oscillatory systems, Phys. Rep. **373,** 247 (2003).

[38] L. Huang, S. M. Soskin, I. A. Khovanov, R. Mannella, K. Ninios, and H. B. Chan, Frequency stabilization and noise-induced spectral narrowing in resonators with zero dispersion, Nat. Commun. **10,** 3930 (2019).